# Zeeman Effect of the Purely Cubic Field Fluorescence Line of MgO:$Cr^{3+}$ Crystals*

S. SUGANO,† A. L. SCHAWLOW, AND F. VARSANYI‡
*Bell Telephone Laboratories, Murray Hill, New Jersey*

(Received August 5, 1960)

Both transverse and longitudinal Zeeman effects are studied of the most conspicuous red emission line (14 319 $cm^{-1}$) of a MgO:$Cr^{3+}$ single crystal. The Zeeman patterns are examined experimentally, with a magnetic field parallel to the [001], [110] and [111] axes, with linear polarizations parallel and perpendicular to each direction of the magnetic field and with circular polarizations around the magnetic field.

Comparing these patterns with those theoretically calculated under the reasonable assumptions, it is found that the line is a magnetic dipole radiation due to the $t_2^3\,{}^2E \rightarrow t_2^3\,{}^4A_2$ transition of chormium ions with purely cubic environments. It is also found that the Jahn-Teller coupling of chromophoric electrons and lattice in the excited state may be ignored in explaining the Zeeman effect.

## I. INTRODUCTION

DETAILED analyses of very narrow optical lines based on the crystal field theory have been successfully applied to corundum crystals containing chromium[1] and vanadium[2] impurities. The electronic transitions responsible for these lines involve a change of spin, but no change of parity, and thus violate both the spin and parity selection rules. However, in these crystals, the local crystal field at the transition metal ion sites is nearly cubic but it has a fairly large trigonal component belonging to both even and odd parities. This trigonal component causes an admixture of states of odd-parity, leading to a small electric dipole strength for the otherwise forbidden transitions in collaboration with spin-orbit interaction, and we know that such a mechanism characterizes the nature of the lines, especially their Zeeman effects.[3]

Another crystal which presents very narrow spectral lines due to chromium impurities is magnesium oxide.[4] Paramagnetic resonance studies of this crystal have revealed that a dominating part of the chromium ions present is exposed to a purely cubic field while the others are exposed to tetragonal and rhombic fields.[5] Therefore, the most conspicuous red fluorescence line located at 14 319 $cm^{-1}$ may be considered to be due to chromium ions with purely cubic environment. This is further evidenced by the isotropic behavior of the Zeeman splitting of this line as a sharp Zeeman pattern can be obtained even with a powdered sample.

It is known since Deutschbein's observation that the MgO:$Cr^{3+}$ fluorescence spectrum in the red region has several sharp lines and some broader ones besides the above-mentioned 14 319 $cm^{-1}$ line. We also observed many rather sharp lines but only the strongest one mentioned above seemed to have an isotropic $g$ factor. Elucidation of the cause of the other lines is not attempted here, although it is indispensable in understanding fully the MgO:$Cr^{3+}$ spectrum: these lines are being investigated in our laboratory in collaboration with Wood.[6]

The study of the purely cubic field optical line is interesting because it belongs to the simplest system without involving any odd crystal field, which causes electric dipole transitions in the case of corundum crystals. Therefore, the appearance of the optical line ascribed to this otherwise forbidden transition has to be explained either by an electric dipole transition slightly released by the asymmetric distortion of the system due to lattice vibrations, or by a magnetic dipole one. Studying the Zeeman effect experimentally and theoretically, it will be shown that a magnetic dipole transition is responsible for the line.

Another interest of this study comes from the expectation that the Jahn-Teller effect[7] might be seen in the Zeeman patterns of the line. This is because, for chromium ions in the cubic field, there remains a degeneracy other than the Kramers degeneracy in the excited state which will be responsible for the line as mentioned below. Contrary to this expectation, however, it will be clarified that we can explain the Zeeman effect without taking this effect into account.

It will be assumed here that the line in question arises from the transition $t_2^3\,{}^2E \rightarrow t_2^3\,{}^4A_2$. There is another excited state, namely $t_2^3\,{}^2T_1$ which is considered to fall in the spectral region where the line is observed. The reason for the ${}^2T_1$ state being excluded in the assignment is partly as follows; the observed

* A preliminary account of this work was presented at the Symposium on Molecular Structure and Spectroscopy, Ohio State University, June 13–17, 1960 (unpublished).

† On leave from the Department of Physics, Tokyo University, Tokyo, Japan.

‡ Present address: Department of Physics, the Johns Hopkins University, Baltimore, Maryland.

[1] S. Sugano and Y. Tanabe, J. Phys. Soc. (Japan) **13**, 880 (1958); S. Sugano and I. Tsujikawa, J. Phys. Soc. (Japan) **13**, 899 (1958).

[2] M. H. L. Pryce and W. A. Runciman, Discussions Faraday Soc. No. 26, 34 (1958).

[3] S. Sugano, Suppl. Progr. Theoret. Phys. (Kyoto) **14**, 66 (1960).

[4] O. Deutschbein, Ann. phys. **14**, 712, 729 (1932).

[5] W. Low, Phys. Rev. **105**, 801 (1957); J. E. Wertz and P. Auzins, Phys. Rev. **106**, 484 (1957); J. H. E. Griffiths and J. W. Orton, Proc. Phys. Soc. (London) **73**, 948 (1959).

[6] A. L. Schawlow and D. L. Wood (to be published).

[7] W. Moffitt and A. D. Liehr, Phys. Rev. **106**, 1195 (1957); H. C. Longuet-Higgins, U. Öpik, M. H. L. Pryce, and R. A. Sack, Proc. Roy. Soc. (London) **A244**, 1 (1958).

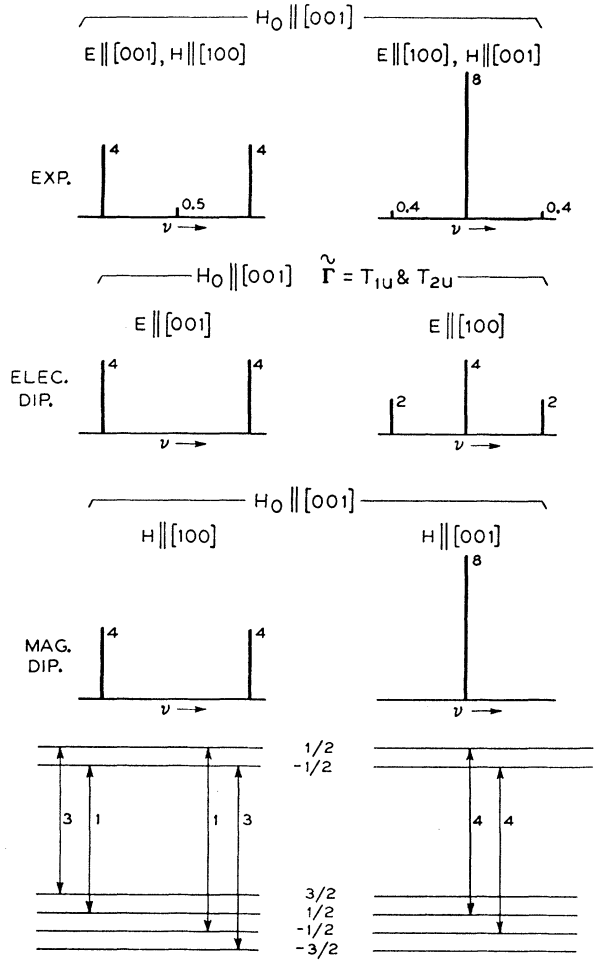


FIG. 1. The experimental and calculated Zeeman patterns (elec. dip. and mag. dip.) with $H_0 \| [001]$. The transition diagram is associated with the mag. dip. Zeeman patterns. $\tilde{\Gamma}$ stands for the mode of the coupled vibration in the electric dipole transitions. The intensities of the experimental Zeeman patterns are the relative ones in each pattern and not normalized.

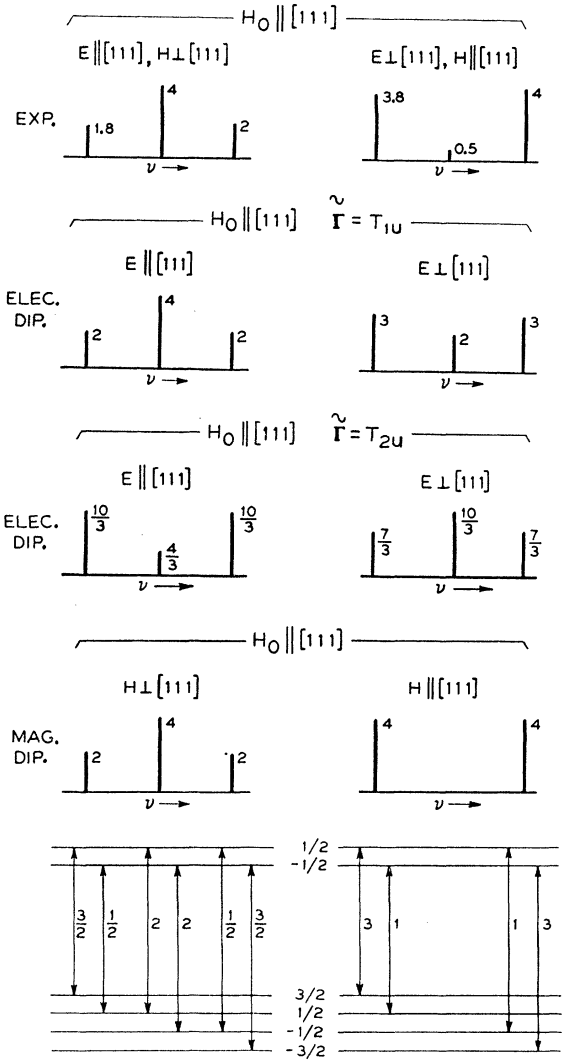


FIG. 2. The similar figure to Fig. 1, with $H_0 \| [111]$.

Zeeman patterns of the line show that the excited state splits into two Zeeman levels and the spectroscopic splitting factor is very close to the spin-only value, while the splitting factors of the $^2T_1$ states[8] are expected to be largely deviated from a spin-only value because of the nonvanishing contribution of the orbital angular momentum. This assumption will be confirmed by comparing the theoretical Zeeman patterns with the experimental ones.

## II. EXPERIMENTAL PROCEDURE

A transparent, light greenish single crystal of MgO containing about 0.1% chromium impurity was used in these experiments. A MgO crystal has the NaCl type crystal structure and can be cleaved along the (100) plane fairly easily. Thus a small cube with the edges of about 3 mm length was obtained. Finally we polished down the cubes suitably to get the (110) and (111) faces.

The quantitative measurements of the fluorescence spectrum were carried out by using both photographic and photoelectric techniques. All the measurements were made at 77°K.[9] The applied magnetic field was up to 30 000 oe. The fluorescence was excited by the simultaneous use of several tungsten microscope lamps with appropriate blue filters, which transmitted radiation in the region of the broad band absorption of the sample. A matching sharp-cut red filter was

[8] This level is slightly split into two sublevels by the spin-orbit coupling even in absence of a magnetic field.

[9] Some measurements were made at 4.2°K to confirm the ratio of the transition probabilities from the $\frac{1}{2}$ and $-\frac{1}{2}$ levels of the excited state. Assuming thermal equilibrium between up and down spins in the excited state, the observed ratios are in good agreement with the theoretical ones.

used on the spectrograph slit to cut out completely the exciting light.

In order to obtain the polarization data, a microscope polarizer sheet or a circular-polarizer constructed from a polaroid and a $\lambda/4$-plate was placed between the sample and a focusing lens. Thus the depolarizing effect of the lens was eliminated. Unfortunately, however, the Dewar vessel seemed to induce some undesirable effects and thus will be the main source of the observed slight polarization mixing.

For photographic measurements a Bausch and Lomb Dual Grating Spectrograph was used with a 55 000 lines per inch grating giving a dispersion of about 1.5 A per mm in the investigated region. Kodak *I-L* plates were used for the detection of the fluorescence. They were calibrated and microphotometered for intensities.

During the course of the work, a high-resolution photoelectric spectrometer became available (manufactured by the Jarrell-Ash Company and based on the design of Fastie, Crosswhite, and Gloersen[10]). When used with a good replica of a 7500 line per inch Harrison grating, a resolution of about 1/30 $cm^{-1}$ in the investigated region can be achieved. Results obtained with this instrument agreed well with those obtained photographically in cases where comparisons were made. Thus obtained intensity patterns are shown at the tops of Figs. 1, 2, and 3 for the transverse Zeeman effects, and at the bottoms of Figs. 5, 6, and 7 for the longitudinal Zeeman effects. It should be noticed that the absolute unit of the intensities is chosen arbitrarily for each kind of the Zeeman patterns.

## III. CALCULATIONS OF THE ZEEMAN PATTERNS ASSUMING ELECTRIC DIPOLE TRANSITIONS

The chromium lattice site in MgO crystals is a center of symmetry. Therefore, we can expect an electric dipole transition only when the electronic transition accompanies simultaneous excitation of odd-parity crystal vibrations, which will slightly distort the local crystalline field. Then the dipole strengths of the electric dipole transitions[11] from the $^4A_2$ ground state to the $^2E$ excited state are given by the following formula[3];

$$\mathfrak{S}\,(^4A_2M_se_2:n\rightarrow{}^2E\bar{M}_s\bar{\gamma}:\bar{n})$$
$$=|\sum_{\gamma'}(^4A_2M_se_2:n|\mathfrak{P}|^4T_2M_s\gamma':\bar{n})$$
$$\times(^4T_2M_s\gamma':\bar{n}|V_{so}|^2E\bar{M}_s\bar{\gamma}:\bar{n})|^2$$
$$\times[W(^2E)-W(^4T_2)]^{-2},\quad(1)$$

here the first element is given by

$$(^4A_2M_se_2:n|\mathfrak{P}|^4T_2M_s\gamma':\bar{n})$$
$$=\sum_{\alpha_u'\Gamma_u'\gamma_u'}(^4A_2:n|\mathbf{P}|\alpha_u'{}^4\Gamma_u'\gamma_u':n)$$
$$\times(\alpha_u'{}^4\Gamma_u'\gamma_u':n|V_{ov}|^4T_2\gamma':\bar{n})$$
$$\times[W(^4T_2)-W(\alpha_u'\Gamma_u')]^{-1}$$
$$+\sum_{\alpha_u''\Gamma_u''\gamma_u''}(^4A_2:n|V_{ov}|\alpha_u''{}^4\Gamma_u''\gamma_u'':\bar{n})$$
$$\times(\alpha_u''{}^4\Gamma_u''\gamma_u'':\bar{n}|\mathbf{P}|^4T_2\gamma':\bar{n})$$
$$\times[W(^4A_2)-W(\alpha_u''{}^4\Gamma_u'')]^{-1},\quad(2)$$

where $V_{so}$ denotes the spin-orbit interaction, $V_{ov}$ the

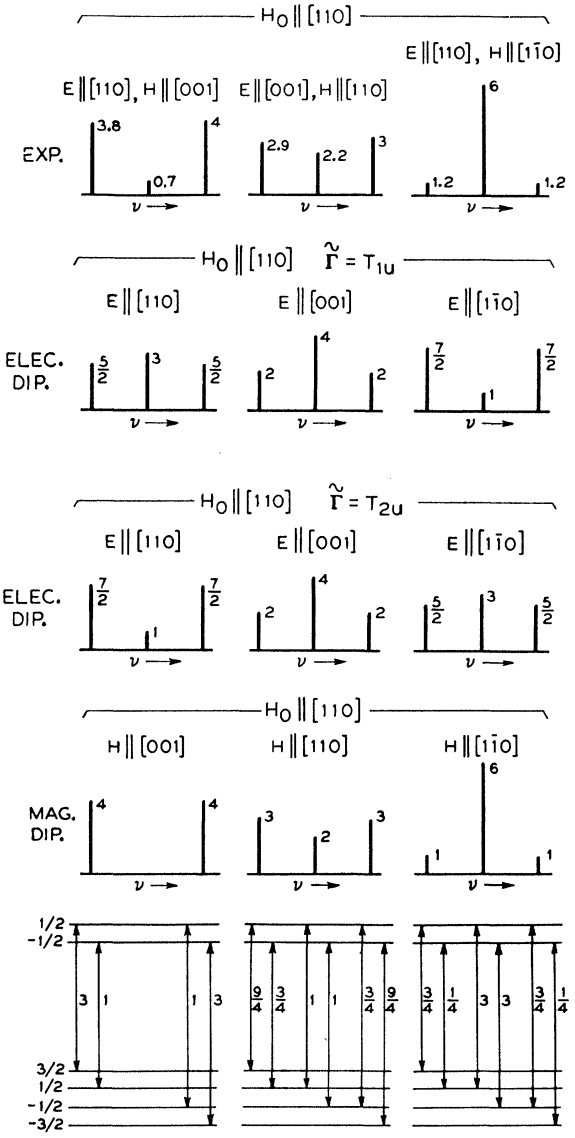


FIG. 3. The similar figure to Fig. 1, with $H_0\|[110]$.

[10] W. G. Fastie, H. M. Crosswhite, and P. Gloersen, J. Opt. Soc. Am. 48, 106 (1958).

[11] In the calculation of dipole strengths, we use throughout this paper a language and formalism for absorption instead of those for emission because this makes no difference in our approximation and it is more familiar to the reader.

coupling of chromophoric electrons to odd vibrations and $\mathbf{P}$ the electric dipole $\sum e\mathbf{r}_i$. $W(\alpha S\Gamma)$ is the energy of the $\alpha S\Gamma$ state, and $n$ and $\bar{n}$ stand for a set of vibrational quantum numbers of the states. The term $V_{ov}$ may be expanded as follows:

$$V_{ov}=\sum_{\tilde{\Gamma}\tilde{\gamma}} V(\tilde{\Gamma}\tilde{\gamma})\cdot Q(\tilde{\Gamma}\tilde{\gamma}), \tag{3}$$

where $Q(\tilde{\Gamma}\tilde{\gamma})$ is the normal coordinate of the lattice vibration belonging to the $\tilde{\Gamma}\tilde{\gamma}$ mode.

We assume here that the coupling of chromophoric electrons is sufficiently large only with the vibrations within the framework of the Cr-$O_6$ octahedron, and take the $T_{1u,a}$, $T_{1u,b}$, and $T_{2u}$ modes in the summation over $\tilde{\Gamma}$. Furthermore, we shall assume that the normal coordinates of vibrations are the same in the ground and excited state.[7] Then, in the absorption spectrum at very low temperature, $n$ expresses the state with zero-point vibrations and $\bar{n}$ the state in which a single quantum of the $\tilde{\Gamma}\tilde{\gamma}$ odd vibration is excited. In the case of the emission spectrum, the situation is just reversed.

In the purely cubic field, the orbital degeneracy of the $^2E$ state remains unresolved even in presence of a magnetic field, so that the dipole strength in the expression (1) should be summed over $\bar{\gamma}$.

In the calculation of the Zeeman patterns, it is convenient to quantize the spin in the direction of the applied magnetic field, because the spin of both the ground and excited states in our case always follows the direction of the magnetic field. For this purpose, it is necessary to get the matrix element of the spin-orbit interaction in expression (1) with $M_s$ and $\bar{M}_s$ being quantized in the arbitrary direction. This is achieved by applying the following unitary transformations $U_{mm'}{}^{(j)}(\phi\theta\psi)$ to the spin states in the spin-orbit matrix:

$$U_{mm'}{}^{(j)}=e^{-im\phi}U_{mm'}{}^{(j)}(\theta)e^{-im'\psi}, \tag{4}$$

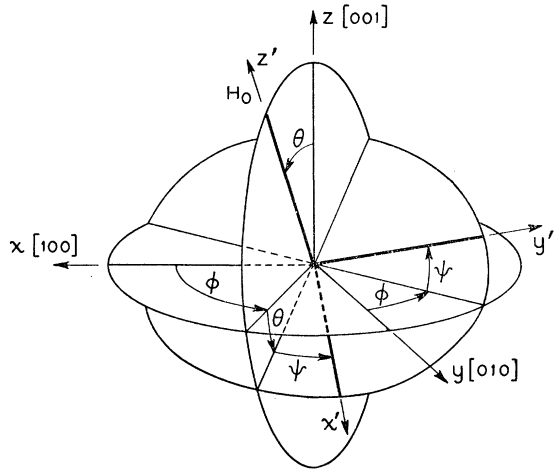


FIG. 4. The relative direction of the applied magnetic field to the crystal axes.

where $U_{mm'}{}^{(\frac{1}{2})}(\theta)$ is given by

| $m$ \ $m'$ | $\frac{1}{2}$ | $-\frac{1}{2}$ |
|---|---|---|
| $\frac{1}{2}$ | $a$ | $-b$ |
| $-\frac{1}{2}$ | $b$ | $a$, |

(5)

and $U_{mm'}{}^{(\frac{3}{2})}(\theta)$ is given by

| $m$ \ $m'$ | $\frac{3}{2}$ | $\frac{1}{2}$ | $-\frac{1}{2}$ | $-\frac{3}{2}$ |
|---|---|---|---|---|
| $\frac{3}{2}$ | $a^3$ | $-\sqrt{3}a^2b$ | $\sqrt{3}ab^2$ | $-b^3$ |
| $\frac{1}{2}$ | $\sqrt{3}a^2b$ | $a(1-3b^2)$ | $b(1-3a^2)$ | $\sqrt{3}ab^2$ |
| $-\frac{1}{2}$ | $\sqrt{3}ab^2$ | $-b(1-3a^2)$ | $a(1-3b^2)$ | $-\sqrt{3}a^2b$ |
| $-\frac{3}{2}$ | $b^3$ | $\sqrt{3}ab^2$ | $\sqrt{3}a^2b$ | $a^3$ . |

(6)

In (5) and (6) we use the abbreviation

$$a=\cos(\theta/2),\quad b=\sin(\theta/2).$$

The transformation angles, $\phi$, $\theta$, and $\psi$ are the Eulerian angles representing the direction of the magnetic field which is described in Fig. 4, and $m$ and $m'$ are the magnetic spin quantum numbers referred to the fixed and rotated systems, respectively. The matrix elements of the spin-orbit interaction thus obtained is given in Table I, in which the orbital part is left referred to the fourfold axes of the crystal.

Now, by using these matrix elements, the calculation of the relative intensities among the Zeeman components, with arbitrary directions of the magnetic field $H_0$ and of the polarization of light $E$, may be performed, if we know what orbitals of the $^4T_2$ state are excited with the given polarization. In order to make comparison with the experiment, the polarizations $E\|[001]$, $E\|[110]$, $E\|[111]$ and $E\perp[111]$ will be considered. From these four cases, all the observed patterns can be derived. For treating the cases of $E\|[111]$ and $E\perp[111]$ with $H_0\|[111]$, it is more convenient to use trigonal bases from the beginning. Since these cases have been already treated in another paper,[3] we shall only quote the result.[12]

From the tables of the Wigner coefficients for a cubic group,[13] the orbitals of the $^4T_2$ state excited for a given polarization are given as follows; for $E\|[001]$,

| the excited orbital $\gamma'$ | the coupled vibration $\tilde{\Gamma}\tilde{\gamma}$ |
|---|---|
| $\xi$ | $T_{1u}\beta$ and $T_{2u}\eta$ |
| $\eta$ | $T_{1u}\alpha$ and $T_{2u}\xi$; |

for $E\|[110]$,

| the excited orbital $\gamma'$ | the coupled vibration $\tilde{\Gamma}\tilde{\gamma}$ |
|---|---|
| $\zeta$ | $T_{1u}(\alpha-\beta)$ and $T_{2u}(\xi+\eta)$ |
| $(\xi-\eta)/\sqrt{2}$ | $T_{1u}\gamma$ |
| $(\xi+\eta)/\sqrt{2}$ | $T_{2u}\zeta$. |

The absolute square of the matrix element

[12] The Zeeman patterns of this case can be obtained from Figs. 4 and 5 of reference 3 by superposing both patterns of $R_1$ and $R_2$.

[13] Y. Tanabe and S. Sugano, J. Phys. Soc. (Japan) **9**, 753 (1954).

TABLE I. The matrix element $(t_2^3\,{}^2E\bar{M}_s\bar{\gamma}|v_{so}|t_2^2e\,{}^4T_2M_s\gamma')$, with $\bar{M}_s$ and $M_s$ being quantized along the direction $(\phi,\theta,\psi)$.

| $\bar{\gamma}$ | $\bar{M}_s$ \ $M_s$ | $\gamma'$ $\frac{3}{2}$ | $\xi$ (or $i\eta$)[a] $\frac{1}{2}$ | $-\frac{1}{2}$ | $-\frac{3}{2}$ | $\zeta$[c] $\frac{3}{2}$ | $\frac{1}{2}$ | $-\frac{1}{2}$ | $-\frac{3}{2}$ |
|---|---|---|---|---|---|---|---|---|---|
| $u$ | $\frac{1}{2}$ | $\sqrt{3}(\pm b^2e^{i\phi}-a^2e^{-i\phi})$ | $2ab(\pm e^{i\phi}+e^{-i\phi})$ | $\pm a^2e^{i\phi}-b^2e^{-i\phi}$ | 0 | 0 | 0 | 0 | 0 |
| | $-\frac{1}{2}$ | 0 | $\pm b^2e^{i\phi}-a^2e^{i\phi}$ | $2ab(\pm e^{i\phi}+e^{-i\phi})$ | $\sqrt{3}(\pm a^2e^{i\phi}-b^2e^{-i\phi})$ | 0 | 0 | 0 | 0 |
| $v$ | $\frac{1}{2}$ | $(b^2e^{i\phi}\mp a^2e^{-i\phi})$ | $(2ab/\sqrt{3})(e^{i\phi}\pm e^{-i\phi})$ | $(1/\sqrt{3})(a^2e^{i\phi}\mp b^2e^{-i\phi})$ | 0 | $\sqrt{3}ab$ | $a^2-b^2$ | $-ab$ | 0 |
| | $-\frac{1}{2}$ | 0 | $(1/\sqrt{3})(b^2e^{i\phi}\mp a^2e^{-i\phi})$ | $(2ab/\sqrt{3})(e^{i\phi}\pm e^{-i\phi})$ | $(a^2e^{i\phi}\mp b^2e^{-i\phi})$ | 0 | $ab$ | $a^2-b^2$ | $-\sqrt{3}ab$ |

[a] Take the lower sign for $i\eta$.
[b] All values tabulated for $\xi$ (or $i\eta$) are to be multiplied by $(-i\xi'/\sqrt{6})$.
[c] All values tabulated for $\zeta$ are to be multiplied by $(2\sqrt{2}i\zeta'/3)$.

$({}^4A_2M_se_2:n|\mathfrak{P}|{}^4T_2M_s\gamma':\tilde{n})$ has a common value for all the above-mentioned excitation so that this value is not important in the discussion of the relative intensities.

The transition probabilities from the Zeeman levels of the ${}^4A_2$ ground state to those of the ${}^2E$ state are thus obtained in an arbitrary unit[14] as given in Table II. In Table II, the magnetic spin quantum numbers $M_s$ and $\bar{M}_s$ are referred to the direction given by $(\phi,\theta,\psi)$, and $A$, $B$, $\lambda$, and $\mu$ are defined as follows:

$$A=\cos\theta, \qquad B=\sin\theta,$$
$$\lambda=\cos(\phi+\pi/4), \qquad \mu=\sin(\phi+\pi/4).$$

The procedure of deriving Zeeman patterns from this table is as follows:

(i) $H_0\|[001]$, $E\|[001]$: The Zeeman pattern is obtained by putting $\theta=0$ in the $E\|[001]$ column.

(ii) $H_0\|[001]$, $E\|[100]$: This is equivalent to the case of $H_0\|[100]$ and $E\|[001]$, so that we put $\theta=\pi/2$ in the $E\|[001]$ column.

(iii) $H_0\|[110]$, $E\|[001]$: The pattern is equivalent to that given in (ii), because the values in the column $E\|[001]$ are independent of $\phi$.

(iv) $H_0\|[110]$, $E\|[110]$: The pattern is obtained by putting $\phi=\pi/4$ and $\theta=\pi/2$ in the $E\|[110]$ column.

(v) $H_0\|[110]$, $E\|[1\bar{1}0]$: This is equivalent to the case of $H_0\|[1\bar{1}0]$ and $E\|[110]$, so that we put $\phi=-\pi/4$ and $\theta=\pi/2$ in the $E\|[110]$ column.

The Zeeman patterns thus obtained are illustrated in Figs. 1, 2, and 3. Comparing these with the observed patterns, it is clear that even qualitative agreement is not obtained.[15] The discrepancy of the $H_0\|[001]$, $E\|[100]$ pattern is fatal, because the observed pattern corresponding to this case is the most characteristic one. Furthermore, if we adopt the $T_{1u}$ mode in order to fit the calculated and experimental patterns in the $H_0\|[111]$ case, we have qualitative discrepancies in the $H_0\|[110]$ case, etc.

[14] The unit is calculated as $\zeta'^2C^2(\tilde{\Gamma}T_2)/\{9[W({}^2E)-W({}^4T_2)]^2\}$, $C(\tilde{\Gamma}T_2)$ being defined in reference 3.

[15] The qualitative disagreement between the observed Zeeman patterns with $H_0\|[110]$, $E\|[110]$, $H\|[001]$ and with $H_0\|[110]$, $E\|[110]$, $H\|[1\bar{1}0]$ also tells us directly that the radiation is not electric dipole, but in our work the latter pattern was supplemented after we took the procedure mentioned here and arrived at the conclusion.

## IV. CALCULATION OF THE ZEEMAN PATTERNS ASSUMING MAGNETIC DIPOLE TRANSITIONS

In the previous section, it was clarified that the electric dipole transitions are unable to explain the observed Zeeman effect. Another possibility to explain the experiment is to assume magnetic dipole transitions.

Magnetic dipole has matrix elements between the ${}^4A_2$ ground state and only one excited state $t_2^2e\,{}^4T_2$. Therefore, a simple calculation of the magnetic dipole strengths is possible that is exact within the $d^3$ configuration. The magnetic dipole strengths polarized in $\gamma_0$ are given by

$$\mathfrak{S}^{\rm mag}({}^4A_2M_se_2\rightarrow{}^2E\bar{M}_s\gamma:\gamma_0)$$
$$=\beta^2|\textstyle\sum_{\gamma'}({}^4A_2M_se_2|\mathbf{M}(\gamma_0)|{}^4T_2M_s\gamma')$$
$$\times({}^4T_2M_s\gamma'|V_{so}|{}^2E\bar{M}_s\bar{\gamma})|^2[W({}^4T_2)-W({}^2E)]^{-2}, \quad (7)$$

where

$$\mathbf{M}=-\textstyle\sum_i(\boldsymbol{l}_i+2\mathbf{s}_i), \quad (8)$$

$\gamma_0$ denoting a component of $\mathbf{M}$ and $\beta$ being the Bohr magneton. The polarized (in $\gamma_0$) oscillator strength of the line in absence of a magnetic field, $\bar{f}^{\rm mag}$, is given by[3]

$$\bar{f}^{\rm mag}(\gamma_0)=\frac{\pi\bar{\sigma}}{3\beta^2c}\sum_{M_s,\bar{M}_s,\bar{\gamma}}\mathfrak{S}^{\rm mag}(\gamma_0), \quad (9)$$

where $\bar{\sigma}$ is the wave number of the spectral line and $c$

TABLE II. Electric dipole strengths of the transition $t_2^3\,{}^4A_2M_s\leftrightarrow t_2^3\,E\bar{M}_s$, where the magnetic spin quantum numbers $M_s$ and $\bar{M}_s$ are referred to the direction of the magnetic field expressed by $\theta$, $\phi$, and $\psi$: $A=\cos\theta$, $B=\sin\theta$, $\lambda=\cos(\phi+\pi/4)$ and $\mu=\sin(\phi+\pi/4)$. The upper and lower signs of $M_s$ correspond to the upper and lower signs of $\bar{M}_s$, respectively. $\tilde{\Gamma}$ is the coupled vibrational mode. The unit is taken arbitrary.

| ${}^4A_2M_s$ \ ${}^2E\bar{M}_s$ | $E\|[001]$ $\tilde{\Gamma}=T_{1u},T_{2u}$ $\pm\frac{1}{2}$ | $E\|[110]$[a] $\tilde{\Gamma}=T_{1u}$ $\pm\frac{1}{2}$ |
|---|---|---|
| $\pm\frac{3}{2}$ | $3(A^2+1)$ | $\frac{3}{4}[(3\mu^2+\lambda^2)A^2+4B^2+(3\lambda^2+\mu^2)]$ |
| $\pm\frac{1}{2}$ | $4B^2$ | $4A^2+(3\mu^2+\lambda^2)B^2$ |
| $\mp\frac{1}{2}$ | $(A^2+1)$ | $\frac{1}{4}[(3\mu^2+\lambda^2)A^2+4B^2+(3\lambda^2+\mu^2)]$ |
| $\mp\frac{3}{2}$ | 0 | 0 |
| Sum | 8 | 8 |

[a] The values for $E\|[110]$, $\tilde{\Gamma}=T_{2u}$ are obtained by interchanging $\lambda$ and $\mu$ in those for $E\|[110]$, $\tilde{\Gamma}=T_{1u}$.

TABLE III. Magnetic dipole strengths of the transition $t_2^3\,{}^4A_2M_s \leftrightarrow t_2^3\,{}^2E\bar{M}_s$. The notations are the same as those given in Table II.

| ${}^4A_2M_s$ \ ${}^2E\bar{M}_s$ | $H\|[001]$ $\pm\frac{1}{2}$ | $H\|[110]$ $\pm\frac{1}{2}$ |
|---|---|---|
| $\pm\frac{3}{2}$ | $3B^2$ | $\frac{3}{4}[3(A^2\lambda^2+\mu^2)+(A^2\mu^2+\lambda^2)]$ |
| $\pm\frac{1}{2}$ | $4A^2$ | $3B^2\lambda^2+B^2\mu^2$ |
| $\mp\frac{1}{2}$ | $B^2$ | $\frac{1}{4}[3(A^2\lambda^2+\mu^2)+(A^2\mu^2+\lambda^2)]$ |
| $\mp\frac{3}{2}$ | 0 | 0 |
| Sum | 4 | 4 |

is the velocity of light. The $\sum \mathfrak{S}^{\mathrm{mag}}(\gamma_0)$ is found to be

$$\sum_{M_s,\bar{M}_s,\gamma} \mathfrak{S}^{\mathrm{mag}}(\gamma_0)$$

$$=64k'^2\zeta'^2\beta^2/\{27[W({}^4T_2)-W({}^2E)]^2\}, \quad (10)$$

$$k'=(1/\sqrt{2})(t_2x_+|\,l_z\,|eu_+), \quad (11)$$

$$\zeta'=-\sqrt{2}(t_2\tfrac{1}{2}x_+|\,V_{\mathrm{so}}\,|e\tfrac{1}{2}u_+), \quad (12)$$

where $x_+$ and $u_+$ are trigonal bases of the $T_2$ and $E$ representation.[1] Assuming the values, $\bar{\sigma}=14\,000$ cm$^{-1}$, $W({}^4T_2)-W({}^2E)=4000$ cm$^{-1}$, $k'=1$ and $\zeta'=250$ cm$^{-1}$ (slightly less than $\zeta=273$ cm$^{-1}$ of a free chromium ion), we find

$$\bar{f}^{\mathrm{mag}}(\gamma_0)=5.5\times10^{-9}. \quad (13)$$

For unpolarized light we should multiply by a factor of two. The value thus obtained seems not too small to be observed. The assumption of the magnetic dipole transitions is also consistent with the fact that the absorption line of MgO:$Cr^{3+}$ is much weaker compared with that of ruby.[6]

The calculation of the Zeeman patterns is similar to that of the previous case. Let us consider the cases where the magnetic vector of light, $H$, is parallel to the [001] and [110] directions. From the tables of the Wigner coefficient for cubic group, we know that, for $H\|[001]$ and $H\|[110]$, the $\zeta$ and $(\xi+\eta)/\sqrt{2}$ orbitals of the ${}^4T_2$ state are, respectively, excited, and $|({}^4A_2M_se_2|\mathbf{M}|{}^4T_2M_s\gamma')|^2$ with the above $\gamma'$ is a common factor in the transition probabilities. Then, by using the spin-orbit matrix given in Table I, the transition probabilities in an arbitrary unit are given in Table III.

TABLE IV. Magnetic dipole strengths of the transition $t_2^3\,{}^4A_2\bar{M}_s \leftrightarrow t_2^3\,{}^2E\bar{M}_s$, with $H_0\|[111]$.

| ${}^4A_2M_s$ \ ${}^2E\bar{M}_s$ | $\frac{1}{2}$ | $-\frac{1}{2}$ |
|---|---|---|
| $\frac{3}{2}$ | $3(\|\hat{k}^0\|^2+\|\hat{k}^+\|^2)$ | 0 |
| $\frac{1}{2}$ | $2(\|\hat{k}^+\|^2+\|\hat{k}^-\|^2)$ | $(\|\hat{k}^0\|^2+\|\hat{k}^+\|^2)$ |
| $-\frac{1}{2}$ | $(\|\hat{k}^0\|^2+\|\hat{k}^-\|^2)$ | $2(\|\hat{k}^+\|^2+\|\hat{k}^-\|^2)$ |
| $-\frac{3}{2}$ | 0 | $3(\|\hat{k}^0\|^2+\|\hat{k}^-\|^2)$ |
| Sum | 8 | 8 |

For the cases of $H\|[111]$ and $H\perp[111]$ with $H_0\|[111]$, the transition probabilities are calculated by using in (7) trigonal bases from the beginning. We adopt the following form for a magnetic dipole vector;

$$\mathbf{M}=-M_+\hat{k}^--M_-\hat{k}^++M_0\hat{k}^0, \quad (14)$$

where $\hat{k}^+$, $\hat{k}^-$, and $\hat{k}^0$ are defined by

$$\hat{k}^+=-(1/\sqrt{2})(\hat{\imath}+i\hat{\jmath}),$$
$$\hat{k}^-=(1/\sqrt{2})(\hat{\imath}-i\hat{\jmath}). \quad (15)$$
$$\hat{k}^0=\hat{k},$$

$\hat{\imath}$ and $\hat{\jmath}$ being the mutually orthogonal unit vectors in the plane perpendicular to the [111] axis and $\hat{k}$ parallel to the same axis. From the tables of the Wigner coefficient in the trigonal scheme,[16] we know that, for the polarizations in the directions of $\hat{k}^+$, $\hat{k}^-$, and $\hat{k}^0$, $x_+$, $x_-$, and $x_0$ orbitals of the ${}^4T_2$ state are, respectively, excited, and $|({}^4A_2M_se_2|\mathbf{M}|{}^4T_2M_sM')|^2$ is a common factor in the transition probabilities. The necessary matrix elements of the spin-orbit interaction in the trigonal scheme are already known,[1] so that the dipole strength (7) is now easily evaluated. The dipole strength for the linear polarization $H\|[111]$ is given by the coefficient of $|\hat{k}|^2$, and that for the linear polarization $H\perp[111]$ is given by the coefficient of $|\hat{\imath}|^2$ or $|\hat{\jmath}|^2$. The result is given in Table IV.

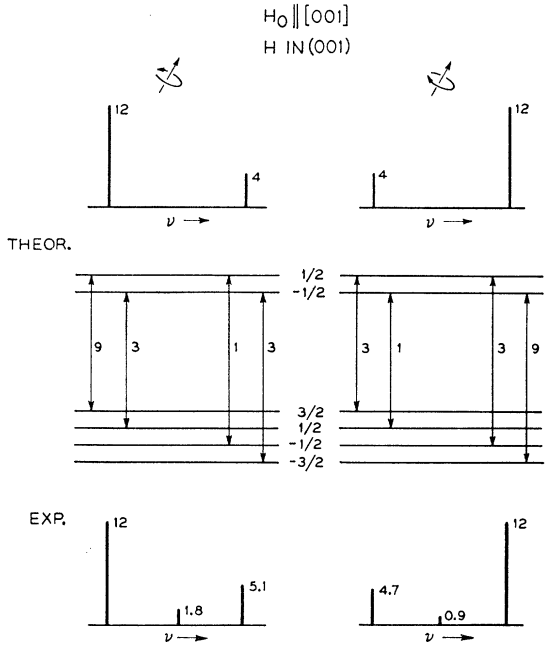


FIG. 5. The experimental and theoretical longitudinal Zeeman patterns with $H_0\|[001]$ in terms of circular polarization. The straight arrow shows the direction of the applied magnetic field, and the circulating one around the straight arrow indicates the direction of the rotating magnetic vector of the radiation.

[16] Y. Tanabe and H. Kamimura, J. Phys. Soc. (Japan) **13**, 394 (1958).

TABLE V. Magnetic dipole strengths of the transition $t_2^3\,{}^4A_2M_s \leftrightarrow t_2^3\,{}^2E\bar{M}_s$, in terms of a circular polarization in the (001) plane. The notations are the same as those given in Table II. $H$ in (001).

| ${}^4A_2M_s$ \ ${}^2E\bar{M}_s$ | $\frac{1}{2}$ | $-\frac{1}{2}$ |
|---|---|---|
| $\frac{3}{2}$ | $(9a^4+3b^4)\lvert\hat{k}^+\rvert^2+(9b^4+3a^4)\lvert\hat{k}^-\rvert^2$ | 0 |
| $\frac{1}{2}$ | $16a^2b^2(\lvert\hat{k}^+\rvert^2+\lvert\hat{k}^-\rvert^2)$ | $(3a^4+b^4)\lvert\hat{k}^+\rvert^2+(3b^4+a^4)\lvert k^-\rvert^2$ |
| $-\frac{1}{2}$ | $(3b^4+a^4)\lvert\hat{k}^+\rvert^2+(3a^4+b^4)\lvert\hat{k}^-\rvert^2$ | $16a^2b^2(\lvert\hat{k}^+\rvert^2+\lvert\hat{k}^-\rvert^2)$ |
| $-\frac{3}{2}$ | 0 | $(9b^4+3a^4)\lvert\hat{k}^+\rvert^2+(9a^4+3b^4)\lvert\hat{k}^-\rvert^2$ |
| Sum | 8 | 8 |

Taking the same procedure as shown in the previous section with the use of Table III, and Table IV, the calculated Zeeman patterns are illustrated in Figs. 1, 2, and 3 together with the transition diagrams. The agreement between the experimental and theoretical results is very good in this case. Slight discrepancies, that the observed central components of the $H_0\|[110]$, $H\|[001]$ and $H_0\|[111]$, $H\|[111]$ cases are not vanishing as expected theoretically, are mainly due to some depolarization effect induced in the cryostat. The observed slight enhancement of the intensity of the short-wavelength side component compared to that of the opposite side component is qualitatively explained by assuming a thermal equilibrium between up and down spins in the excited state.

In view of the nice agreement obtained, it may be concluded that orbital degeneracies of the excited Zeeman levels are not resolved beyond the linewidth, that is, the Jahn-Teller coupling between chromophoric electrons and lattice plays no apparent role in the excited state. This might be due to the smallness of the coupling, that is inherent to the system with a half-filled shell configuration, such as $t_2^3$.

## V. THE LONGITUDINAL ZEEMAN EFFECT

In the previous sections, we have been concerned only with the transverse Zeeman effect of the spectrum. This is sufficient to establish the magnetic dipole character of the transition. However, further studies on the longitudinal Zeeman effect will be also interesting in view of confirming the assignment and of developing combined microwave-optical experiments similar to those by Geschwind, Collins, and Schawlow.[17] Therefore, we shall examine, in this section, the longitudinal Zeeman effect of the magnetic dipole transition in terms of circular polarizations for the cases of $H_0\|[001]$, $H_0\|[111]$ and $H_0\|[110]$.

In treating the cases of $H_0\|[001]$ and $H_0\|[110]$, we calculate dipole strengths of the magnetic dipole transitions with circular polarizations in the planes of (001) and (110), respectively, leaving the direction of the magnetic field arbitrary.

For the circular polarization in the (001) plane, the magnetic vector may be written as

$$\mathbf{M}=-M_+\hat{k}^- - M_-\hat{k}^+, \tag{16}$$

in which $\hat{k}^+$ and $\hat{k}^-$ have the same forms as those given in (15) but, in this case, unit vectors $\hat{\imath}$ and $\hat{\jmath}$ are along the [100] and [010] axes, respectively. The components $M_\pm$ are defined as follows,

$$\begin{aligned} M_+&=-(1/\sqrt{2})(M_x+iM_y),\\ M_-&=(1/\sqrt{2})(M_x-iM_y). \end{aligned} \tag{17}$$

It is easy to see from the Wigner coefficients for a cubic group that the orbitals $-(\xi+i\eta)/\sqrt{2}$ and $(\xi-i\eta)/\sqrt{2}$ of the ${}^4T_2$ state are excited with equal probabilities by the $\hat{k}^+$ and $\hat{k}^-$ polarized light, respectively. Then, by the use of the matrix element given in Table I, the result in Table V is obtained. The intensities of counter-clock and clockwise circular polarizations of the magnetic vector of light are given by the coefficients of $\lvert\hat{k}^+\rvert^2$ and $\lvert\hat{k}^-\rvert^2$, respectively,

TABLE VI. Magnetic dipole strengths of the transition $t_2^3\,{}^4A_2M_s \leftrightarrow t_2^3\,{}^2E\bar{M}_s$, in terms of a circular polarization in the $(1\bar{1}0)$ plane. The notations are the same as those given in Table II. $H$ in $(1\bar{1}0)$.

| ${}^4A_2\bar{M}_s$ \ ${}^2E\bar{M}_s$ | $\frac{1}{2}$ | $-\frac{1}{2}$ |
|---|---|---|
| $\frac{3}{2}$ | $3[3A^2\lambda^2+3\mu^2+A^2\mu^2+(\lambda\pm 2B)^2]\lvert\hat{k}^\pm\rvert^2$ | 0 |
| $\frac{1}{2}$ | $4[3B^2\lambda^2+B^2\mu^2+4A^2]\lvert\hat{k}^\pm\rvert^2$ | $[3A^2\lambda^2+3\mu^2+A^2\mu^2+(\lambda\pm 2B)^2]\lvert\hat{k}^\pm\rvert^2$ |
| $-\frac{1}{2}$ | $[3A^2\lambda^2+3\mu^2+A^2\mu^2+(\lambda\mp 2B)^2]\lvert\hat{k}^\pm\rvert^2$ | $4[3B^2\lambda^2+B^2\mu^2+4A^2]\lvert\hat{k}^\pm\rvert^2$ |
| $-\frac{3}{2}$ | 0 | $3[3A^2\lambda^2+3\mu^2+A^2\mu^2+(\lambda\mp 2B)^2]\lvert\hat{k}^\pm\rvert^2$ |
| Sum | 8 | 8 |

[17] S. Geschwind, R. J. Collins, and A. L. Schawlow, Phys. Rev. Letters **3**, 545 (1959).

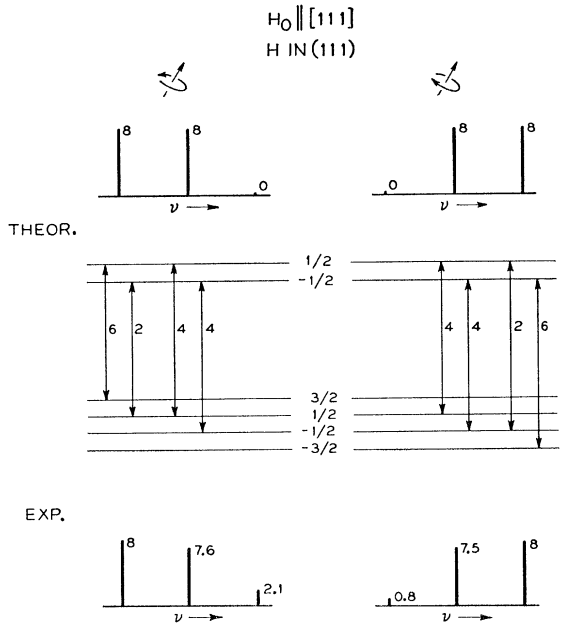


FIG. 6. The similar figure to Fig. 5, with $H_0\|[111]$.

when the magnetic field is coming to our eyes. For $H_0\|[001]$, inserting the values $a=1$ and $b=0$ in Table V we obtain the Zeeman patterns illustrated in Fig. 5. It will be interesting to notice the following observation done during the course of the calculation: for both circular polarizations, the stronger component is always the radiation from the $u$ $(3z^2-x^2)$-orbital and the weaker one from the $v$ $(x^2-y^2)$-orbital. Since the respective radiations from the $u$- and $v$-orbitals have

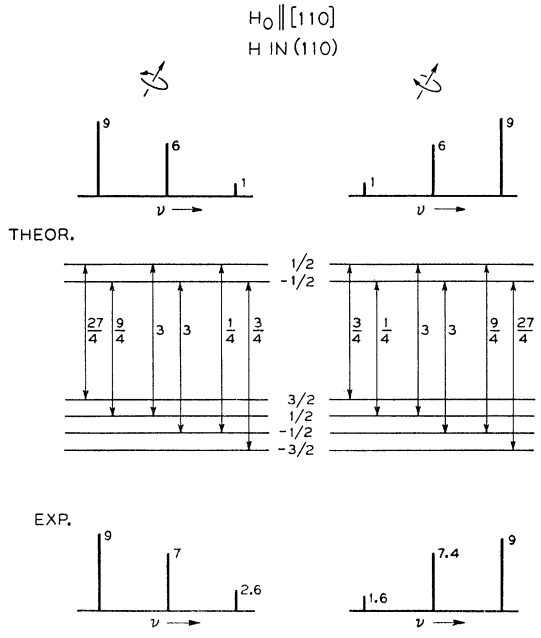


FIG. 7. The similar figure to Fig. 5, with $H_0\|[110]$.

no phase correlation, the Zeeman component is not elliptically polarized as usually expected from the figure but only the mixture of radiations with the circular polarizations in the opposite direction and with the different intensities. This is consistent with the symmetry consideration that no elliptical polarization can exist in the (001) plane because of the fourfold symmetry around the [001] axis.

The treatment of the circular polarization in the (110) plane can be replaced by the treatment of that in the $(1\bar{1}0)$ plane. Here, we will concern with the latter because of its formal simplicity. The magnetic dipole vector in the $(1\bar{1}0)$ plane may be written in the same form as (16) with the unit vectors $\hat{\imath}$ and $\hat{\jmath}$ along the [110] and [001] axes, respectively, and with the

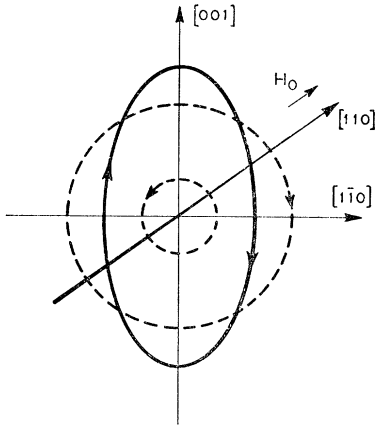


FIG. 8. The expected mode of the elliptical polarization in the longer wavelength side component of the longitudinal Zeeman pattern with $H_0\|[110]$ (Fig. 7). The broken circles indicate the circularly rotating magnetic vectors in the opposite directions, which have fixed relative phases and different amplitudes. The solid ellipse is obtained by superposing two circulating vectors mentioned above.

components $M_\pm$ as follows,

$$M_+=-(1/\sqrt{2})[(1/\sqrt{2})(M_x+M_y)+iM_z],$$
$$M_-=(1/\sqrt{2})[(1/\sqrt{2})(M_x+M_y)-iM_z]. \quad (18)$$

In this case, the orbitals $-(1/\sqrt{2})[(1/\sqrt{2})(\xi+\eta)+i\zeta]$ and $(1/\sqrt{2})[(1/\sqrt{2})(\xi+\eta)-i\zeta]$ of the $^4T_2$ state are excited with equal probabilities by the $\hat{k}^+$ and $\hat{k}^-$ polarized light, respectively. Then, the transition probabilities in Table VI are obtained. For $H_0\|[1\bar{1}0]$, inserting the values $\lambda=1$, $\mu=0$, $A=0$ and $B=1$ in Table VI, we obtain the Zeeman patterns illustrated in Fig. 7.[18] It will be interesting to mention the following facts found during the course of the calculation: all the side components are radiations from the $v$-orbital and the central component is that from the $u$-orbital. Then, the phases of the two circularly polarized radiations within the side component should be cor-

[18] In this figure we return to the case of $H_0\|[110]$, $H$ in the (110) plane.

related to each other, so that we can expect elliptically polarized radiations for the side components. The predicted elliptical polarization mode of the longer wavelength side component is illustrated in Fig. 8. The central component is linearly polarized along the $[1\bar{1}0]$ axis ($H\|[1\bar{1}0]$) when the magnetic field is applied along the [110] axis.

The longitudinal Zeeman effect with $H_0\|[111]$ is obtained from the results given in Table IV. The Zeeman patterns are visualized in Fig. 6. The characteristic feature of this result is such that the central component is linearly polarized in the (111) plane while the side components are circularly polarized in the opposite sense to each other in the same plane.

The agreement of these calculated longitudinal Zeeman patterns with the experimental ones is very good in all cases as expected.


### ACKNOWLEDGMENTS

We would like to express our sincere thanks to D. L. Wood for showing us his unpublished experimental results on the MgO:$Cr^{3+}$ spectrum. W. B. Mims kindly allowed us to use some magnesium oxide crystals which had been given to him by Dr. G. R. Finlay of the Norton Company. We are indebted to A. M. Clogston for several helpful discussions and to G. E. Devlin for extensive assistance with the experiments.


PHYSICAL REVIEW VOLUME 120, NUMBER 6 DECEMBER 15, 1960

# Thomas-Fermi Technique for Determining Wave Functions for Alkali Atoms with Excited Valence Electrons*

HARVEY J. BRUDNER† AND SIDNEY BOROWITZ
*Department of Physics, New York University, Washington Square, New York, New York, and Institute of Mathematical Sciences, New York University, New York, New York*

(Received July 15, 1960)

A technique has been developed for the calculation of excited state, one-electron wave functions based on the Thomas-Fermi statistical theory of the atom. This technique is applied to heavy alkali atoms for which Hartree-type solutions are complex and difficult to obtain. The Thomas-Fermi differential system for the alkali positive ions is accurately solved utilizing Milne's method, and the results are summarized. This Thomas-Fermi core potential is then used as a central field in the Schrödinger equation together with the Heisenberg type of polarization energy correction. Angular dependence is assumed to be capable of separation, and two basic techniques for solving the radial Schrödinger equation are discussed, one due to Ridley, the other to Biermann and Lübeck. The general approach permits correction for penetration of the excited electron's orbital. The Biermann and Lübeck type solution also allows for the inclusion of a qualitative correction for exchange. The techniques are applied to the potassium atom with an excited valence electron in the 6*s* state. The results are encouraging when compared with a Biermann and Lübeck type calculation using a Hartree central potential done by Villars. The 7*s* state of the cesium atom which has not been obtained by Hartree central potential is also computed.

## I. INTRODUCTION

THE only systematic approach to the calculation of atomic structure and properties is via the Hartree[1] or Hartree-Fock[2] approximation. However, there are limitations to these calculations. Their numerical complexity makes it difficult to obtain an overall physical picture of the atom. Only isolated solutions are possible in these approximations and for heavier atoms the numerical complexity of the self-consistent iterations makes the calculations for atomic structure all but impossible.

There are additional complications which arise when attempting to calculate the structure of excited states since one requires that the wave functions used be orthogonal to all lower states, and it is sometimes impossible to obtain solutions with this requirement.

For those states for which Hartree or Hartree-Fock one-electron wave functions cannot be obtained, one can use a somewhat cruder approximation which has the advantage of simplicity, namely the Thomas-Fermi model.[3,4] The basic assumptions in this model, however, require that we investigate only the ground-state configurations. Some attempts have been made by Latter[5] to investigate the excited states of an electron in the Thomas-Fermi central potential. This is of course an approximation to the description of excited states

* This research has been supported by the Geophysics Research Directorate of the Air Force Cambridge Research Center, Air Research and Development Command, the Office of Ordnance Research, and the Office of Naval Research.

† Present address: College of Physicians and Surgeons, Columbia University, 630 West 168 Street, New York 32, New York.

[1] D. R. Hartree, Proc. Cambridge Phil. Soc. **23**, 542 (1926).
[2] V. Fock, Z. Physik **61**, 126 (1930).
[3] L. H. Thomas, Proc. Cambridge Phil. Soc. **23**, 542 (1926).
[4] E. Fermi, Rend. accad. nazl. Lincei **6**, 602 (1927); Z. Physik **48**, 73 (1928).
[5] R. Latter, Phys. Rev. **90**, 510 (1955).